RSC Advances

PAPER

View Article Online
View Journal | View Issue

Cite this: *RSC Adv.*, 2022, **12**, 25060

A portable smartphone-based detection of glyphosate based on inhibiting peroxidase-like activity of heptanoic acid/Prussian blue decorated Fe_3O_4 nanoparticles†

Dan Chen,[ab] Chunqiong Wang,[b] Dezhi Yang,[c] Huimin Deng,[d] Qiulan Li,[c] Li Chen,[e] Gaokun Zhao,[f] Junli Shi,[f] Ke Zhang*[b] and Yaling Yang*[c]

The rapid and onsite detection of glyphosate in tobacco products is still a great challenge. In this study, a novel smartphone-assisted sensing platform for the detection of glyphosate has been successfully proposed through the peroxidase-like activity of Fe_3O_4-based nanozyme. Heptanoic acid/Prussian blue (PB) decorated Fe_3O_4 nanoparticles (Fe_3O_4@C_7/PB) could catalyze and oxidize 2,2′-azino-bis(3-ethylbenzothiazoline-6-sulfonic acid) (ABTS, colorless) into a steel blue colored product in the presence of hydrogen peroxide. Glyphosate could specifically inhibit the peroxidase-like activity of Fe_3O_4@C_7/PB by occupying the active site, thereby the glyphosate detection could be accomplished within 10 min by monitoring the color change of ABTS. This study has developed a smartphone-based portable detection platform for online analysis of glyphosate with a detection limit of 0.1 μg mL^{-1}. The absorbance response curve of glyphosate showed good linearity in the concentration range of 0.125–15 μg mL^{-1} at 415, 647, and 730 nm. Moreover, by employing a co-precipitation technology and inhibiting the peroxidase-like activity, the glyphosate analysis would be less affected by the tobacco sample matrix. The nanosensor possesses excellent selectivity and anti-interference ability, which has application value in actual samples for onsite screening.

Received 31st May 2022
Accepted 29th July 2022

DOI: 10.1039/d2ra03382h

rsc.li/rsc-advances

1 Introduction

Glyphosate is a high-efficiency and broad-spectrum non-selective sterilant herbicide, which has been widely used in many fields especially in agriculture for its high conductivity, cost-effectiveness, and systemic killing efficiency.[1,2] Glyphosate has become one of the world's top ranked herbicides and its usage is still on the increase.[3] Although there are a number of factors that alter the solubility and rate of degradation of glyphosate in the substrate, which results in controversy about glyphosate toxicity at present, a large number of residues easily produce chronic potential toxicity to animals and humans through food chain accumulation. Poisoning cases are still reported from time to time.[4–6] As such, China, U.S. Environmental Protection Agency, and the European Union have all set limits for glyphosate residues.[7] Glyphosate is an amino acid herbicide with strong polarity, high solubility in water, and insoluble in general organic solvents. Its molecule structure lacks chromogenic and fluorescent groups, and has a strong binding ability with organic compounds in plants which make the direct detection and quantification difficult by traditional analytical techniques. To improve the analytical detection of glyphosate, various derivation method were developed for mass spectrometry,[8] electrochemistry,[9] ion chromatography,[10] and fluorescent spectrometry.[11]

Nanomaterials with bionic enzymes activities (*i.e.* nanozymes) are generally mass-produced at low cost and are stable compared to the natural enzymes and are promising candidates for the detection of pesticides.[12] Colorimetric sensing based on catalytic oxidation of chromogenic substrates, even at trace amounts of target by nanozymes has been reported.[13–15] Detection of pesticides by colorimetric nanozymes is based mostly on the inhibition of nanozymes activity.[16,17] Luo *et al.* proposed a facile colorimetric nanozyme sheet for the rapid detection of glyphosate in agricultural products based on inhibiting peroxidase-like catalytic activity of porous Co_3O_4 nanoplates.[4]

[a]*Peking University, School of Materials Science and Engineering, Beijing 100871, China*

[b]*Yunnan Institute of Tobacco Quality Inspection & Supervision, Kunming 650500, China. E-mail: swukirk@126.com*

[c]*Faculty of Life Science and Technology, Kunming University of Science and Technology, Kunming 650500, China. E-mail: yangyl2016@qq.com*

[d]*China National Tobacco Quality Supervision & Test Center, Zhengzhou 450001, China*

[e]*Zhengzhou Tobacco Research Institute of CNTC, Zhengzhou, China*

[f]*Yunnan Academy of Tobacco Agricultural Sciences, Kunming 650021, China*

† Electronic supplementary information (ESI) available. See https://doi.org/10.1039/d2ra03382h

Liu *et al.* developed a system composed of polyethylenimine-capped upconversion nanoparticles, copper(II), hydrogenperoxide and 3,3′,5,5′-tetramethylbenzidine for colorimetric and fluorometric determination of glyphosate.[1] Yan *et al.* established a colorimetric assay for the detection of organophosphorous pesticides by using peroxidase (POD)-mimicking Fe_3O_4 nanoparticles.[18] Since the first report of Fe_3O_4 nanoparticles in 2007, the research scope has rapidly expanded to a large variety of nanomaterials, and the Fe_3O_4 nanoparticles also were decorated with various functional groups to improve the enzymes activities.[19–21] Similar to Fe_3O_4, Prussian blue (PB) also consists of mixed valence states of Fe with high POD-like activity.[22] Therefore, colorimetric and fluorometric sensing platforms have terrific application prospects.

Although the current methods offer high sensitivity for glyphosate analysis, they generally require more complicated sample preparation for complex matrices, which are not suitable for rapid and on-site detection. Moreover, the catalytic activity of nanomaterials is also easily affected by the surrounding conditions for complex samples. To address these problems, some analytical techniques like preprocessing technology and smartphone-assisted sensing platform have been developed.[21] With high-resolution cameras and powerful computing capabilities, comprehensive smartphone platforms have been developed to receive, process, and display data for biochemical or chemical substances detection.[23–25]

Herein, we have established an anti-interference smartphone-assisted nanosensing platform based on the peroxidase-like activity of heptanoic acid and PB decorated Fe_3O_4 nanoparticles (Fe_3O_4@C_7/PB) for glyphosate assay in tobacco. The potential problem of glyphosate assay in tobacco products is the false-negative results caused by the complex matrix addressed in this study. The as-synthesized Fe_3O_4@C_7/PB exhibited excellent peroxidase-like activity compared to Fe_3O_4, which was evaluated using 2,2′-azino-bis (3-ethylbenzothiazoline-6-sulfonic acid) (ABTS) as a substrate in the presence of H_2O_2 (Scheme 1). Furthermore, the catalytic activity of Fe_3O_4@C_7/PB was inhibited even by trace amounts of glyphosate. Glyphosate molecules can occupy the active sites on the surface of porous Fe_3O_4@C_7/PB nanoparticles, which can block the conversion of H_2O_2 to $^{\cdot}OH$, leading to the delicate color change of ABTS. By monitoring the color change of ABTS, the concentration of glyphosate can be detected within 10 min.

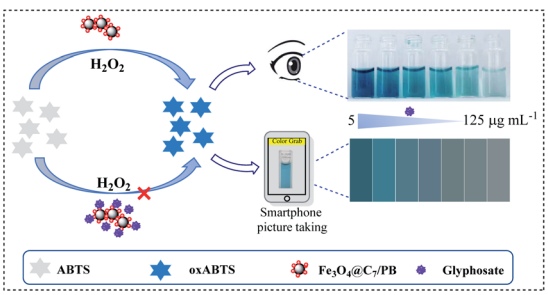

Scheme 1 Schematic of the colorimetric sensors for glyphosate detection.

According to the color changes, the colorimetric quantitative method was developed and employed for glyphosate quantitation by combining the RGB color mode and smartphone technology. Due to its simple operation, low cost, and fast response, the proposed visual method has great potential for on-site evaluation of glyphosate.

2 Experimental section

2.1 Materials

All reagents were of analytical grade, commercially available and used as received unless otherwise indicated. $(NH_4)_2Fe(SO_4)_2\cdot 6H_2O$, heptanoic acid, PB, $FeCl_3\cdot 6H_2O$, $NH_3\cdot H_2O$ (25%w/w), 2,2′-azino-bis(3-ethylbenzothiazoline-6-sulfonic acid) (ABTS), H_2O_2 (30% w/w), glyphosate and other competitive organophosphorus pesticides (OPs) were supplied from Aladdin Industrial Corporation (Shanghai, China). Terephthalic acid (TA) was purchased from the Shanghai Macklin Biochemical Co., Ltd (Shanghai, China). Deionized water used in experiments was prepared by ultra-pure water equipment (18.23 MΩ·cm, UPT-II, Ulupure, China).

2.2 Instrumentation

The morphology and microstructure of the Fe_3O_4@C_7/PB were observed on a TecnaiG2 TF30 transmission electron microscope (TEM) with an accelerating voltage of 200 kV (FEI, USA). UV-vis absorption spectra were determined on a TU-1901 double beam UV-visible spectrophotometer from Beijing Persee General Analysis Instrument Co., Ltd (Persee, China).

2.3 Synthesis of Fe_3O_4@C_7/PB nanoparticles

A one-pot synthesis method was used for the preparation of Fe_3O_4@C_7/PB. Initially, 3.38 g $(NH_4)_2Fe(SO_4)_2\cdot 6H_2O$ and 2.82 g $FeCl_3\cdot 6H_2O$ were dispersed in 80 mL deionized water. The suspension was heated at 80 °C under N_2 atmosphere with vigorous stirring. Then, 200 mg of heptanoic acid (dissolved in 5 mL of acetone), 5 mL of $NH_3\cdot H_2O$ (28%, w/v) and 200 mg PB were added gradually to the solution, respectively. The mixture was kept for 1 h at 80 °C. After cooling down to room temperature, the obtained precipitate was magnetically separated and washed with deionized water followed by ethanol. The precipitate was lyophilized to turn it into a powder. Finally, the acquired powder was redispersed in water and the concentration of nanomaterials was set to 3.24 mg mL^{-1}.

2.4 Kinetic tests of Fe_3O_4@C_7/PB

Under optimal conditions, the kinetic investigation of the POD-like performance of Fe_3O_4@C_7/PB was studied by varying TMB and H_2O_2 concentrations. First, the analysis was studied by using Fe_3O_4@C_7/PB (3.24 mg mL^{-1}) with fixed concentration of H_2O_2 (50 mM) and varied concentration of TMB (0.0625, 0.125, 0.1875, 0.25, 0.3125, 0.375, 0.4375, 0.5, 0.5625, 0.625 mM). Then, H_2O_2 as the substrate, the test was studied by using Fe_3O_4@C_7/PB (3.24 mg mL^{-1}) with fixed concentration of TMB (0.25 mM) and varied concentrations of H_2O_2 (0.625, 1.25,

1.875, 2.5, 3.125, 3.75). The kinetic parameters were calculated according to the Michaelis–Menten equation:

$$1/V = \frac{K_m}{V_{max} \times 1/[S]} + 1/V_{max}$$

where V is the initial velocity, V_{max} is the maximal reaction velocity, [S] is the concentration of substrate, and K_m is the Michaelis constant. The K_m value and V_{max} value of the POD-like activities of Fe_3O_4@C_7/PB, with TMB and H_2O_2 as substrates, were calculated respectively.

2.5 Peroxidase-like catalytic activity of Fe_3O_4@C_7/PB

The peroxidase-like activity of Fe_3O_4@C_7/PB was investigated through employing it to catalyze some chromogenic reactions. Typically, 50 μL of 5 mM ABTS solution, 50 μL (30%) H_2O_2 solution and 50 μL of 1 mg mL^{-1} Fe_3O_4@C_7/PB solution were added to 2.5 mL of 0.1 M NaAc-HAc buffer (pH 2.0). The UV-vis spectra and absorbance values were recorded at a fixed wavelength (416 nm) for analysis.

2.6 Smartphone-based detection of the glyphosate

The detection experiment was carried out in an aqueous medium. First, 50 μL of 5 mM ABTS solution, 50 μL (30%) H_2O_2 solution and 50 μL of 1 mg mL^{-1} Fe_3O_4@C_7/PB solution were added to the prepared sample. Then, 0.1 M NaAc-HAc buffer (pH 2.0) was added to adjust the volume to 2.5 mL. After the color changed, the images were captured by the camera of the smartphone. The obtained color images of different glyphosate concentrations were instantaneously converted by an installed iOS application (APP) called "Color Picker APP" into digital values regarding red (R), green (G), and blue (B) color channels for the onsite quantitative analysis of glyphosate. Finally, inhibition efficiency (IE, %) was applied to assess the inhibitory effects and calculate the glyphosate content. Inhibition efficiency (%) was calculated by the following equation: IE (%) = $(A_0 - A_g)/A_0 \times 100$, where A_g and A_0 represented the absorbance of the Fe_3O_4@C_7/PB–ABTS - H_2O_2 system at 416 nm in the presence and absence of glyphosate, respectively. The limit of detection (LOD) was determined by the 3σ rule. All colorimetric glyphosate measurements were conducted with three replicates.

2.7 Sample pretreatment

For pretreatment of tobacco samples, 1 g of sample powder was added in 30 mL of deionized water containing 1 mL of NaOH (1 M). After 15 min of ultrasonication, the obtained yellow solution was centrifuged at 8000 rpm for 5 min. The supernatant was stored at 4 °C for subsequent decolorization experiments.

The extract was decolorized by the co-precipitation method. Briefly, 300 μL of $Al(OH)_3$ (0.33 M) was added in 2 mL of extract. After mixing, the solution was mixed with 300 μL of NaOH (1 M) and vortex for 30 s. Then, the mixed solution was centrifuged at 6000 rpm for 5 min. The upper glyphosate extract is used for nanozyme inhibition analysis.

In order to avoid the presence of glyphosate in the yellow precipitate, the study has been conducted to reduce the loss of glyphosate through secondary precipitation. 1 mL of deionized water was added into yellow precipitate. After stirring for 1 min, 300 μL of HCl (1 M) was used to dissolve the precipitate. Then, 300 μL of NaOH (1 M) was added for secondary precipitation. After centrifugation, the supernatants of the two extractions were combined and stored at 4 °C for subsequent analysis.

3 Results and discussion

3.1 Characterization of Fe_3O_4@C_7/PB

The TEM image shown in Fig. 1A and B revealed a core–shell structure of Fe_3O_4@C_7 and Fe_3O_4@C_7/PB, respectively. After modification with PB, the particles tended to be slightly larger. The crystalline structures of Fe_3O_4@C_7/PB were identified by XRD analysis (Fig. 1C). The FTIR spectra (Fig. 1D) of AuNPs/CDs and Fe_3O_4@C_7/PB showed IR peaks at 2084 cm^{-1} and 1412 cm^{-1} assigning to the γ(C≡N) stretching mode of PB.[26] The diffraction peaks with 2θ of 17.5°, 24.8°, 39.7° and 51.0° were observed, corresponding to the diffraction plane of 200, 220, 400 and 440 respectively. The high-resolution XPS spectra of Fe 2p, C 1s (284 eV), and N 1s (401.2 eV) were fitted Fe_3O_4@C_7/PB and templating organic moiety (Fig. 1E). The fine Fe 2p XPS (Fig. 1F) provides peaks that can be well assigned to Fe^{3+} $2p_{1/2}$, Fe^{2+} $2p_{1/2}$, Fe^{3+} $2p_{3/2}$ and Fe^{2+} $2p_{3/2}$, verifying the mixed valence states of Fe in the collected products. The prepared Fe_3O_4@C_7/PB was stabilized against agglomeration by a monolayer of PB. This may due to the decorated PB on the surface of Fe_3O_4@C_7. However, the size increases only a little

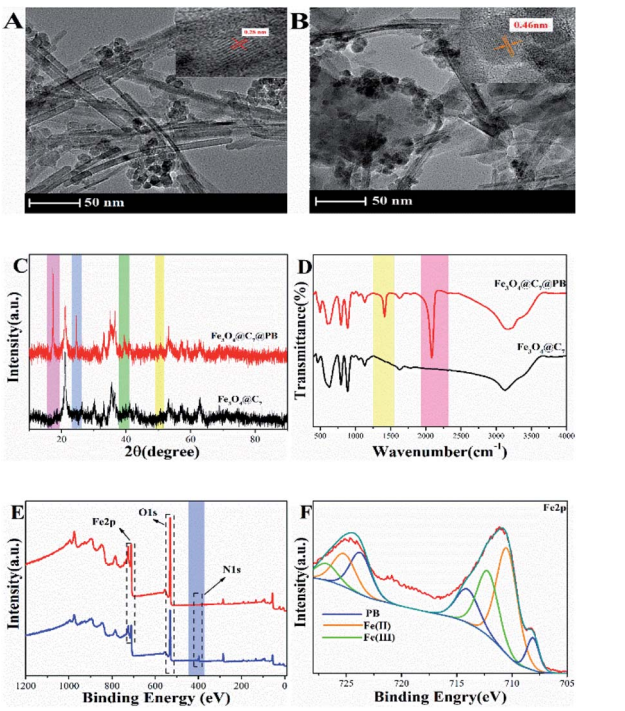

Fig. 1 TEM image of the prepared Fe_3O_4@C_7 (A) and Fe_3O_4@C_7/PB (B); XRD patterns of Fe_3O_4@C_7 and Fe_3O_4@C_7/PB (C); FTIR spectra of Fe_3O_4@C_7 and Fe_3O_4@C_7/PB (D); Survey XPS spectra of Fe_3O_4@C_7 and Fe_3O_4@C_7/PB (E); Core-level spectrum of Fe 2p in Fe_3O_4@C_7/PB composites (F).

with increasing PB which may related to the surface decomposition of Fe_3O_4@C_7 in the reaction process.

3.2 Peroxidase-like activity of Fe_3O_4@C_7/PB

The catalytic performance of the prepared Fe_3O_4@C_7/PB on peroxidase substrates such as TMB and ABTS was evaluated. As shown in Fig. 2A, green (TMB) or steel blue (ABTS) color was observed when the Fe_3O_4@C_7/PB reacted with H_2O_2 at room temperature. An obvious color response for TMB (from colorless to green) and ABTS (from colorless to steel blue) with a maximum absorption peak at 650 nm and 730 nm was observed. In acidic buffer, Fe_3O_4@C_7/PB showed the highest activity on ABTS (~5.0 times) compared with TMB chromogen (Fig. 2A). Due to the excellent affinity and sensitivity of Fe_3O_4@C_7/PB towards ABTS, we selected ABTS as the chromogenic tool for peroxidase–mimic activity for further quantitative smartphone-based analytical assays. In the absence of H_2O_2, the characteristic peaks at 650 nm and 730 nm were not observed (Fig. 2A), which illustrated that the Fe_3O_4@C_7/PB shows peroxidase-like activity. As shown in Fig. 2B, if Fe_3O_4@C_7/PB is pretreated with glyphosate before being introduced into the TMB/H_2O_2 solution, the PODs activity of the Fe_3O_4@C_7/PB is unreversible inhibited by glyphosate.

Although the affinity and sensitivity of Fe_3O_4@C_7/PB towards TBM was observed to be low, the catalytic activity of Fe_3O_4, Fe_3O_4@C_7 and Fe_3O_4@C_7/PB on TMB was also investigated. As can be seen from the Fig. 2C and D, the POD-like activity of the materials presents the following order: Fe_3O_4 < Fe_3O_4@C_7 < Fe_3O_4@C_7/PB. These results indicated that the modification of PB could significantly improve the enzymatic activity of Fe_3O_4@C_7 due to Fenton reaction produces more hydroxyl radicals, so, improving the sensitivity and linear range of the method to the detection of glyphosate.

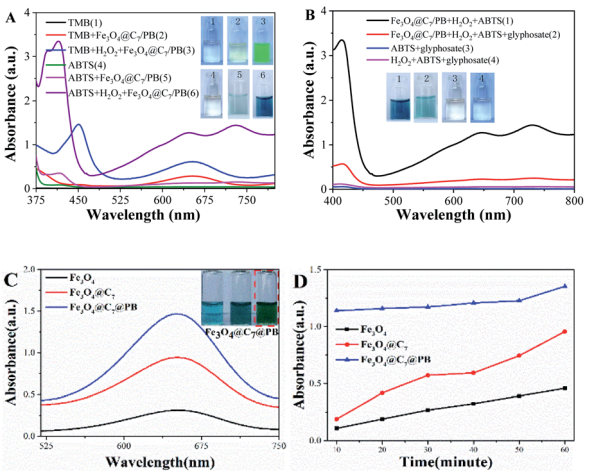

Fig. 2 UV–vis absorbance spectra of the catalytic activity of Fe_3O_4@C_7/PB to TMB and ABTS (A), and the inhibition of glyphosate on different system (B); The catalytic activity of three different materials (Fe_3O_4, Fe_3O_4@C_7 and Fe_3O_4@C_7/PB) on TMB (C); UV absorption spectra of the oxidation of TMB in the presence of Fe_3O_4, Fe_3O_4@C_7 and Fe_3O_4@C_7/PB (D).

To further assess the peroxidase-mimicking catalytic efficiency of Fe_3O_4@C_7/PB, the enzyme kinetic constants (K_m) and the maximum rate (V_{max}) were obtained to measure the enzyme efficiency (Fig. 3). TMB is commonly used for evaluating POD-like activity comparing with natural enzymes. In this study, using H_2O_2 and TMB as substrates, the K_m of Fe_3O_4@C_7 and Fe_3O_4@C_7/PB were 1.392 mM and 0.683 mM for H_2O_2, 1.284 mM and 0.344 mM for TMB, respectively, which were lower than that of horseradish peroxidase (HRP), suggesting that Fe_3O_4@C_7/PB exhibited a higher affinity toward the substrates than to HRP. This may be owing to the existence of more "active sites" on the surface of the Fe_3O_4@C_7/PB. The detailed kinetics parameters are listed in Table 1.

To investigate the effect of glyphosate on peroxidase-like activity of Fe_3O_4@C_7/PB, the absorption spectra of different

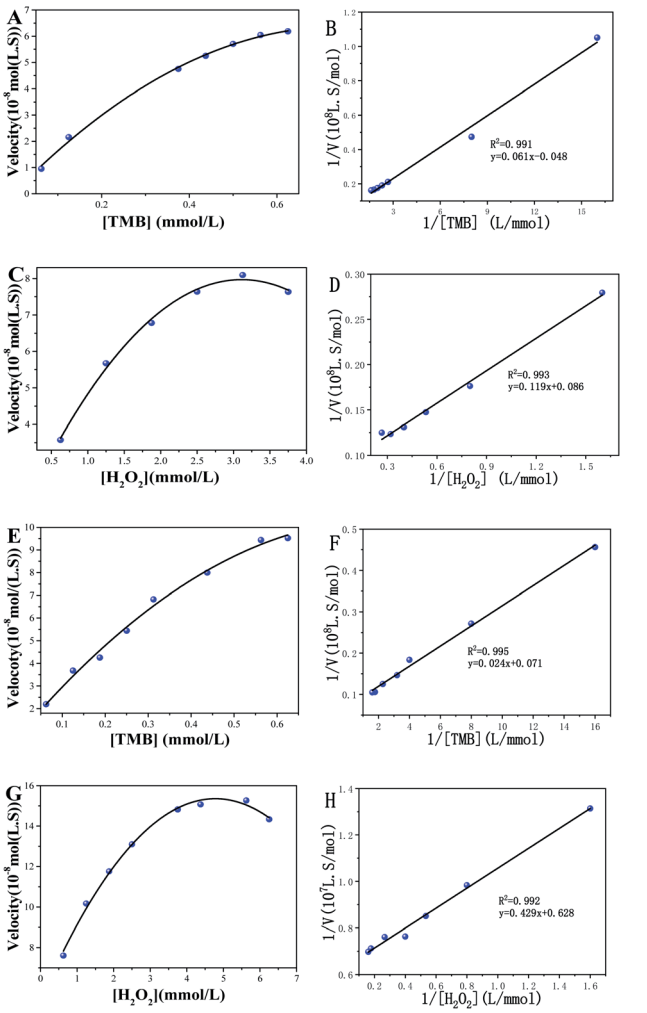

Fig. 3 Steady-state kinetic analysis of Fe_3O_4@C_7 and Fe_3O_4@C_7@PB Peroxidase mimetic. Fe_3O_4@C_7: (A) Curve of velocity against the TMB concentration in the presence of H_2O_2. (C) Curve of velocity against the H_2O_2 concentration in the presence of TMB. (B and D) Double-reciprocal plots of (A and C). Fe_3O_4@C_7@PB: (E) Curve of velocity against the TMB concentration in the presence of H_2O_2. (G) Curve of velocity against the H_2O_2 concentration in the presence of TMB. (F and H) Double-reciprocal plots of (A and C).

Table 1 Comparison of the apparent Michaelis–Menten constant (K_m) and maximum reaction rate (V_{max}) of different NPs

	K_m(mM)		V_{max} (10^{-8}M·s^{-1})	
Catalyst	TMB	H_2O_2	TMB	H_2O_2
Fe_3O_4@C_7	1.284	1.392	21.04	11.65
Fe_3O_4@C_7/PB	0.344	0.683	14.13	15.93
HRP	0.434	3.702	10.00	8.71

systems were measured (Fig. 2B). After the addition of glyphosate, the absorption peak at 730 nm in Fe_3O_4@C_7/PB + H_2O_2 + ABTS + glyphosate was significantly reduced. There is no absorption peak in ABTS + glyphosate and H_2O_2 + ABTS + glyphosate systems, which revealed that glyphosate could not catalytic oxidation of ABTS discoloration and the peroxidase-like activity of Fe_3O_4@C_7/PB could be inhibited by glyphosate. Therefore, the inhibition of Fe_3O_4@C_7/PB enzyme activity could be developed for glyphosate detection.

3.3 Inhibition mechanism of glyphosate on enzyme activity

The Fe_3O_4@C_7/PB nanozyme can promote the ˙OH generation by decomposing H_2O_2, resulting in the oxidation of the substrate ABTS. In the presence of glyphosate, the conversion of H_2O_2 to ˙OH could be interrupted through occupying the active sites on the surface of Fe_3O_4@C_7/PB. To further investigate the inhibition mechanism of glyphosate on catalytic activity of Fe_3O_4@C_7/PB nanozymes, a fluorescence experiment was applied for tracking ˙OH in Fe_3O_4@C_7/PB + H_2O_2 system. Terephthalic acid (TA) was adopted to capture ˙OH because it can become 2-hydroxyterephthalic acid, a fluorescent agent with peak around 430 nm. As illustrated in Fig. 4A, the intensity of fluorescence in Fe_3O_4@C_7/PB + H_2O_2 + glyphosate system was lower than that of Fe_3O_4@C_7/PB + H_2O_2 system, indicating that glyphosate could effectively inhibit the production of ˙OH. In addition, no fluorescence was observed when incubated TA with Fe_3O_4@C_7/PB nanosheets, suggesting clearly the absence of ˙OH. These results confirmed that the peroxidase activity of Fe_3O_4@C_7/PB could be inhibited by glyphosate.

When glyphosate was added in the Fe_3O_4@C_7/PB + ABTS + H_2O_2 system, and the absorbance of the Fe_3O_4@C_7/PB + ABTS + H_2O_2 system decreased (Fig. 4B). While the adsorbed glyphosate on Fe_3O_4@C_7/PB is eluted with different eluents (deionized water, 1%NaOH deionized water, ethanol and 1%NaOH ethanol), the absorbance of the Fe_3O_4@C_7/PB-ABTS-H_2O_2 system was best with 1%NaOH deionized water, indicating that glyphosate adsorbed on Fe_3O_4@C_7/PB was eluted (Fig. 4B). This phenomenon proves our speculation that the active sites of Fe_3O_4@C_7/PB nanozymes were blocked by glyphosate. Surface-enhanced Raman spectroscopy (SERS) was applied to reveal how the active sites were blocked by glyphosate. Au NPs were synthesized according to the reported literature.[27] The SERS spectra showed a much stronger Raman signal intensity of Fe_3O_4@C_7/PB + glyphosate + Au NPs (437, 1344 cm^{-1}) than Au NPs and Fe_3O_4@C_7/PB-Au NPs, and two new signals were observed at 797 and 905 cm^{-1}(Fig. 4C). As can be seen in Fig. S1,† the peak at 440 and 794 cm^{-1} was mainly due to the stretching vibration of the glyphosate molecule (Gaussian 09 programs, density functional theory at the B3LYP/6-31G(d) level). The results showed that a chemical bond could be formed between Fe_3O_4@C_7/PB surface and glyphosate.

3.4 Purification and method optimization

The color interference of tobacco extract has great interference on the colorimetric results. To improve the accuracy and stability of the proposed on-site test sensing platform, co-precipitation technology is used to pretreat the tobacco samples as mentioned in Section 2.7. As shown in Fig. 5A, when $Al(OH)_3$ and NaOH were added, the color interference was eliminated. To test if glyphosate is precipitated by co-precipitation technology, the spiked water and tobacco samples were used to evaluate the co-precipitation purification technology. The glyphosate in the precipitate was also analyzed after being dissolved by 1 mL of HCl (1 M). The precipitation efficiencies of glyphosate were between 1.87 and 3.23%. As shown in Table S1†, the relative standard deviations (RSDs) were in the range of 2.14–4.38%. This result indicated that the

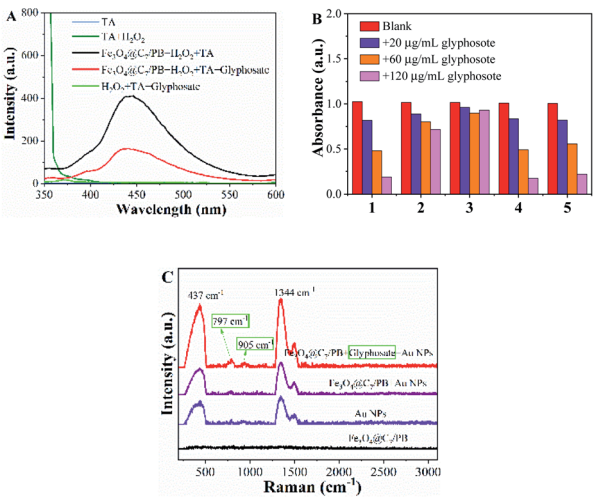

Fig. 4 The fluorescence spectra for the interaction of TA with different systems (A); the elution effect of different eluents on Fe_3O_4@C_7/PB-adsorbed glyphosate (B). 1: Blank; 2: water; 3 : 1%NaOH aqueous solution; 4: Ethanol; 5 : 1%NaOH ethanol solution; Raman spectra of the different system (C).

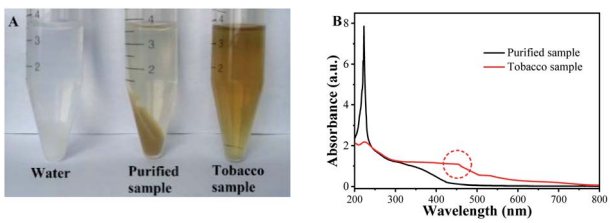

Fig. 5 Purification effect of co-precipitation method on tobacco samples (A); UV-vis absorption spectra of tobacco samples before and after purification (B).

effect of co-precipitation technology on glyphosate detection is almost negligible. After using the co-precipitation method to purify the sample, the absorption peak at 250 nm in tobacco sample was significantly reduced (Fig. 5B). Meanwhile, the background absorbance of the tobacco sample also declined significantly, which illustrated that co-precipitation technology can well eliminate background interference.

The parameters, including the concentrations of Fe_3O_4@C_7/PB, pH, reaction time and substrate concentrations of H_2O_2 and ABTS, were optimized for the ideal analytical performance of the Fe_3O_4@C_7/PB + ABTS + H_2O_2 system. Glyphosate has inhibitory effect on the Fe_3O_4@C_7/PB peroxidase-mimicking activity, which was attributed to the glyphosate molecules occupy the active sites on the surface of porous Fe_3O_4@C_7/PB nanoparticles. Hence, the concentration of Fe_3O_4@C_7/PB plays an important role in the color probe of the detection system. When the concentration of Fe_3O_4@C_7/PB was 12.5 μg mL^{-1}, the chromatic aberration of system colors could easily be identified by the eyes at different glyphosate concentrations. Therefore, the concentration of Fe_3O_4@C_7 was 12.5 μg mL^{-1} in follow-up experiments. Then, to obtain optimal experimental results, the pH, reaction time, the substrate concentrations of ABTS and H_2O_2 were optimized. As shown in Fig. S2,† 10 min of reaction time, pH = 2, 2 mM of H_2O_2 concentration and 0.2 mM of ABTS were selected for the ensuing experiments.

3.5 Assay performance toward glyphosate

The peroxidase-like activity of Fe_3O_4@C_7/PB can promote the decomposition of H_2O_2 into hydroxyl radicals (˙OH), which directly oxidize ABTS to form steelblue products with three characteristic absorption peaks in 416 nm, 647 nm and 730 nm. With an increase in the glyphosate concentration (Fig. 6A and B), the absorbance at 416 nm, 647 nm and 730 nm gradually decreased, which was proportional to the glyphosate concentration, exhibiting linear relationship in the range of 0.125–15 μg mL^{-1} with a good correlation coefficient ($R > 0.99$) and a 0.1 μg mL^{-1} detection limit.

Specificity and anti-interference ability are the crucial indices to estimate the detection capacity of the peroxidase-like nanozyme-based sensor. As shown in Fig. 7, other common pesticides (a-glyphosate b-ilubendiamide, c-imiprothrin, d-thiacloprid, e-atrazine, f-triphenyl phosphate, g-flumetralin, h-butralin, i-pendimethalin, j-parathion-methyl, k-flucythrinate and l-ziram) and phosphate (PO_4^{3-}, HPO_4^{2-} and $H_2PO_4^-$) were chosen to assess the interference effect. Only glyphosate caused an induced remarkable response in the system, while other pesticides with the same concentration (10.0 mg L^{-1}) had no significant effect (Fig. 7A and B). But inorganic phosphate (IP) can also cause the absorbance to decrease in Fe_3O_4@C_7/PB-ABTS-H_2O_2 system, revealing that the phosphate has an interference to the detection system. To clear up interference of the phosphate, we added calcium chloride ($CaCl_2$) to form insoluble compounds between phosphate and Ca^{2+} to eliminate interference (Fig. 7C and D).

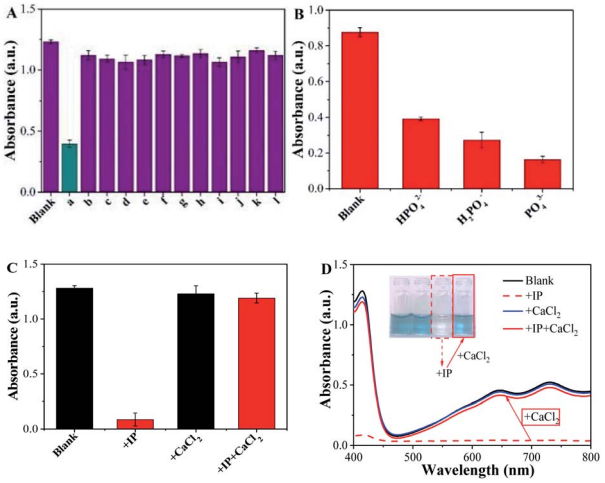

Fig. 7 Specificity of the color sensing platform for glyphosate detection (A); the interference of three kinds of inorganic phosphates, IP (B); the effect of IP, $CaCl_2$ and IP + $CaCl_2$ on the color sensing platform (C); UV-vis absorption spectra of the color sensing platform with IP, $CaCl_2$ and IP + $CaCl_2$, respectively (D). Inset: the color changes of color sensing platform with IP, $CaCl_2$ and IP + $CaCl_2$.

3.6 Smartphone color sensing platform

Due to the significance of on-site testing, portable apparatus and detection should be also considered. We designed a portable smartphone for the on-site detection of glyphosate based on the inhibition of glyphosate on peroxidase activity. By utilizing the system to photograph the reaction solution color with various concentrations of glyphosate and further analyzing through a color recognizer APP installed in the smartphone, the

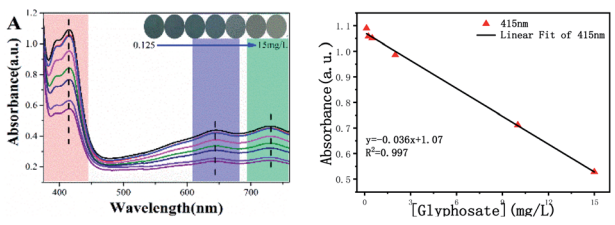

Fig. 6 The colorimetric signal change of the Fe_3O_4@C_7/PB + H_2O_2+ABTS system with different glyphosate concentrations. Inset: the color change of the nanozyme catalytic system (A); linear relationship between the concentration of glyphosate and absorbance (B).

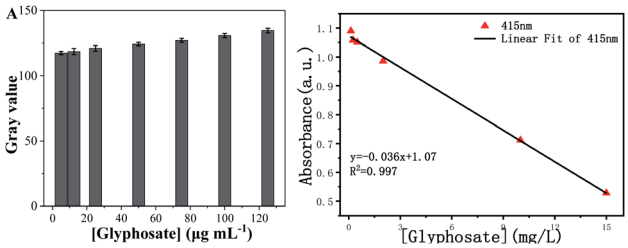

Fig. 8 Smartphone readout gray value *vs.* the concentration of glyphosate (A); and linear relationship between smartphone readout gray value and the concentration of glyphosate (B).

Table 2 Comparison with earlier reported sensing platform for glyphosate detection

Analysis strategy	Materials	Sample	Detection limit	Detection time (min)	Ref.
Smartphone color sensing	Porous Co_3O_4 nanoplates	Cabbage, snow pea, orange	0.175 mg kg^{-1}	10	4
Colorimetric sensor	Copper doped poly(vinyl	Water	0.1 μg mL^{-1}	<1	28
Fluorescent and colorimetric chemosensor	Rhodamine derivative	Agricultural products	4.1 nM	2	29
Colorimetric method	Peroxidase-like activity of Cu^{2+}	—	1 μM	40	30
Electrochemical sensor	Molecularly imprinted polypyrrole nanotubes	Orange juice, rice beverages	1.94 ng mL^{-1}	60	31
Smartphone color sensing	Fe_3O_4@C_7	Tobacco samples	0.5 μg mL^{-1}	10	This work

color changes were transformed into RGB values. As can be seen in Scheme 1, the brightness of the images of the probe solution was inversely correlated with glyphosate concentrations. Coupling with Adobe photoshop CC 2015.5 software, the smartphone readout gray values with different glyphosate concentrations linear relationship in the range of 5–125 μg mL^{-1} ($R^2 = 0.9973$) was acquired in Fig. 8A and B.

The performance of the developed smartphone-assisted sensing platform was compared with other methods in literature. As summarized in Table 2, the detection sensitivity of the proposed method is not as low as the electrochemical sensor, but they have great advantages in on-site testing and detection time.

3.7 Assay of glyphosate in actual samples

Considering that the matrix of tobacco sample is more complicated than general agricultural products, different tobacco products were selected to evaluate the application of the smartphone color sensing platform. As listed in Table S2†, the average recoveries of glyphosate from the spiked actual samples were between 89.44 and 97.10%, and the relative standard deviations were in the range of 1.89–5.38%. Furthermore, the spiked recoveries obtained by the smartphone color sensing platform were very similar to those obtained by GC-MS (China National Standard GB/T 23750–2009). These results revealed that the smartphone color sensing platform had excellent accuracy and repeatability, which had great practical application in the field of rapid detection of glyphosate in tobacco products.

4 Conclusions

In this study, a smartphone-assisted sensing platform with predominant sensitivity and selectivity was constructed for glyphosate assay in complex food matrix as tobacco products. Employing the inhibition of glyphosate on peroxidase-like activity of Fe_3O_4@C_7/PB, a simple but sensitive sensor with good sensitivity has been established. The co-precipitation method was applied to eliminate matrix interference. Furthermore, the results of SERS revealed that the inhibition of enzyme activity was ascribed to the adsorption of glyphosate by nanozyme materials. The established sensor exhibited specific recognition capacity toward glyphosate and showed anti-interference performance against coexisting substances in the tobaccos. The proposed sensing platform integrated the smartphone and color recognizer APP, endowing it with on-site testing in 30 min. What is more, such a smartphone-assisted sensing platform has been triumphantly applied to tobacco samples. These results demonstrated the potential of the established sensing platform for the on-site detection of glyphosate in tobacco samples.

Author contributions

Conceptualisation: D. C., Y. Y., D. Y., C. W.; methodology: D. C., Y. Y.; investigation: D. C., C. W., Q. L., G. Z., H. D., L. C., J. S.; funding acquisition: D. C., K.Z., D. Y., Y. Y., G. Z.; resources: D. C., Y. Y.; writing – original draft: D. C., D. Y., Y. Y.,; writing – review and editing: Y. Y., D. C., D. Y., K. Z.; validation: H.D., L,C., J.S.; visualisation: D. Y., K. Z.; supervision: Y. Y., K. Z.; revision: D. C., Y. Y. All authors reviewed the manuscript.

Conflicts of interest

The authors declare no competing financial interest.

Acknowledgements

This work was greatly supported by the Science and Technology Key Programs of China National Tobacco Corporation Yunnan Company (grant numbers 2020530000241037, 2020530000241034, 2022530000241004) and Analysis and Testing Foundation of Kunming University of Science and Technology (grant numbers 2019P20173118001). Yang Dezhi gratefully acknowledges financial support from Kunming University of Science and Technology high-level talent research platform construction funding (grant numbers 20200097). The authors wish to acknowledge Professor Anyuan Cao, Peking University, for his help in this study.

Notes and references

1 Z. Liu, L. Yang, A. S. Sharma, M. Chen and Q. Chen, *Microchim. Acta*, 2019, **186**, 1–11.
2 C. M. Benbrook, *Environ. Sci. Eur.*, 2016, **28**, 3.

3 J. Gill, N. Sethi and A. Mohan, *Environ. Chem. Lett.*, 2017, **15**, 1–16.
4 D. Luo, X. Huang, B. Liu, W. Zou and Y. Wu, *J. Agric. Food Chem.*, 2021, **69**, 3537–3547.
5 J. P. Myers, M. N. Antoniou, B. Blumberg, L. Carroll, T. Colborn, L. G. Everett, M. Hansen, P. J. Landrigan, B. P. Lanphear, R. Mesnage, L. N. Vandenberg, F. S. Vom Saal, W. V. Welshons and C. M. Benbrook, *Environ. Health: Global Access Sci. Source*, 2016, **15**, 19.
6 T. Tsehaye, S. Bott, I. Cakmak, V. Römheld and G. Neumann, *Eur. J. Agron.*, 2009, **31**, 126–132.
7 S. Wang, B. Liu, D. Yuan and J. Ma, *Talanta*, 2016, **161**, 700–706.
8 M. Motojyuku, T. Saito, K. Akieda, H. Otsuka, I. Yamamoto and S. Inokuchi, *J. Chromatogr. B*, 2008, **875**, 509–514.
9 M. del Carmen Aguirre, S. E. Urreta and C. G. Gomez, *Sens. Actuators, B*, 2019, **284**, 675–683.
10 S. Dovidauskas, I. A. Okada and F. R. Dos Santos, *J. Chromatogr. A*, 2020, **1632**, 461603.
11 A. L. Pérez, G. Tibaldo, G. H. Sánchez, G. G. Siano, N. R. Marsili and A. V. Schenone, *Spectrochim. Acta, Part A*, 2019, **214**, 119–128.
12 S. N. Prasad, V. Bansal and R. Ramanathan, *TrAC, Trends Anal. Chem.*, 2021, **144**, 116429.
13 J. Wu, X. Wang, Q. Wang, Z. Lou, S. Li, Y. Zhu, L. Qin and H. Wei, *Chem. Soc. Rev.*, 2019, **48**, 1004–1076.
14 S. Jin, C. Wu, Z. Ye and Y. Ying, *Sens. Actuators, B*, 2019, **283**, 18–34.
15 Z. Yan, H. Yuan, Q. Zhao, L. Xing, X. Zheng, W. Wang, Y. Zhao, Y. Yu, L. Hu and W. Yao, *Analyst*, 2020, **145**, 3173–3187.
16 Y. Zhu, J. Wu, L. Han, X. Wang, W. Li, H. Guo and H. Wei, *Anal. Chem.*, 2020, **92**, 7444–7452.
17 R. Jin, F. Wang, Q. Li, X. Yan, M. Liu, Y. Chen, W. Zhou, H. Gao, P. Sun and G. Lu, *Sens. Actuators, B*, 2021, **327**, 128922.
18 Y. Xu, T. Yu, X.-Q. Wu, J.-S. Shen and H.-W. Zhang, *RSC Adv.*, 2015, **5**, 101879–101886.
19 L. Gao, K. M. Giglio, J. L. Nelson, H. Sondermann and A. J. Travis, *Nanoscale*, 2014, **6**, 2588–2593.
20 B. C. Yan, J. Cao, J. Liu, Y. Gu, Z. Xu, D. Li and L. Gao, *ACS Biomater. Sci. Eng.*, 2020, **7**, 299–310.
21 Z. Chen, J.-J. Yin, Y.-T. Zhou, Y. Zhang, L. Song, M. Song, S. Hu and N. Gu, *ACS Nano*, 2012, **6**, 4001–4012.
22 X. Niu, Y. He, W. Zhang, X. Li, F. Qiu and J. Pan, *Sens. Actuators, B*, 2018, **256**, 151–159.
23 L. Jia, X. Chen, J. Xu, L. Zhang, S. Guo, N. Bi and T. Zhu, *J. Hazard. Mater.*, 2021, **402**, 123776.
24 H. Zhao, F. Liu, W. Xie, T.-C. Zhou, J. OuYang, L. Jin, H. Li, C.-Y. Zhao, L. Zhang and J. Wei, *Sens. Actuators, B*, 2021, **327**, 128899.
25 D. Lou, Q. Pang, X. Pei, S. Dong, S. Li, W.-q. Tan and L. Ma, *Biosens. Bioelectron.*, 2020, **162**, 112275.
26 T. Wang, Y. Fu, L. Chai, L. Chao, L. Bu, Y. Meng, C. Chen, M. Ma, Q. Xie and S. Yao, *Chemistry*, 2014, **20**, 2623–2630.
27 H. L. a. Z. Z. Mingming Han, *Molecules*, 2020, **25**, 4662.
28 L. K. S. De Almeida, S. Chigome, N. Torto, C. L. Frost and B. I. Pletschke, *Sens. Actuators, B*, 2015, **206**, 357–363.
29 J. Guan, J. Yang, Y. Zhang, X. Zhang, H. Deng, J. Xu, J. Wang and M. S. Yuan, *Talanta*, 2021, **224**, 121834.
30 Y. Chang, Z. Zhe, J. Hao, W. Yang and J. Tang, *Sens. Actuators, B*, 2016, **228**, 410–415.
31 S. Ding, Z. Lyu, S. Li, X. Ruan, M. Fei, Y. Zhou, X. Niu, W. Zhu, D. Du and Y. Lin, *Biosens. Bioelectron.*, 2021, **191**, 113434.